

MiniGPT-3D: Efficiently Aligning 3D Point Clouds with Large Language Models using 2D Priors

Yuan Tang¹ Xu Han¹ Xianzhi Li^{†1} Qiao Yu¹ Yixue Hao¹ Long Hu¹ Min Chen²
¹ Huazhong University of Science and Technology ² South China University of Technology [†] Corresponding author
 {yuan_tang, xhanxu, xzli, qiaoyu_epic, yixuehao, hulong}@hust.edu.cn minchen@ieee.org

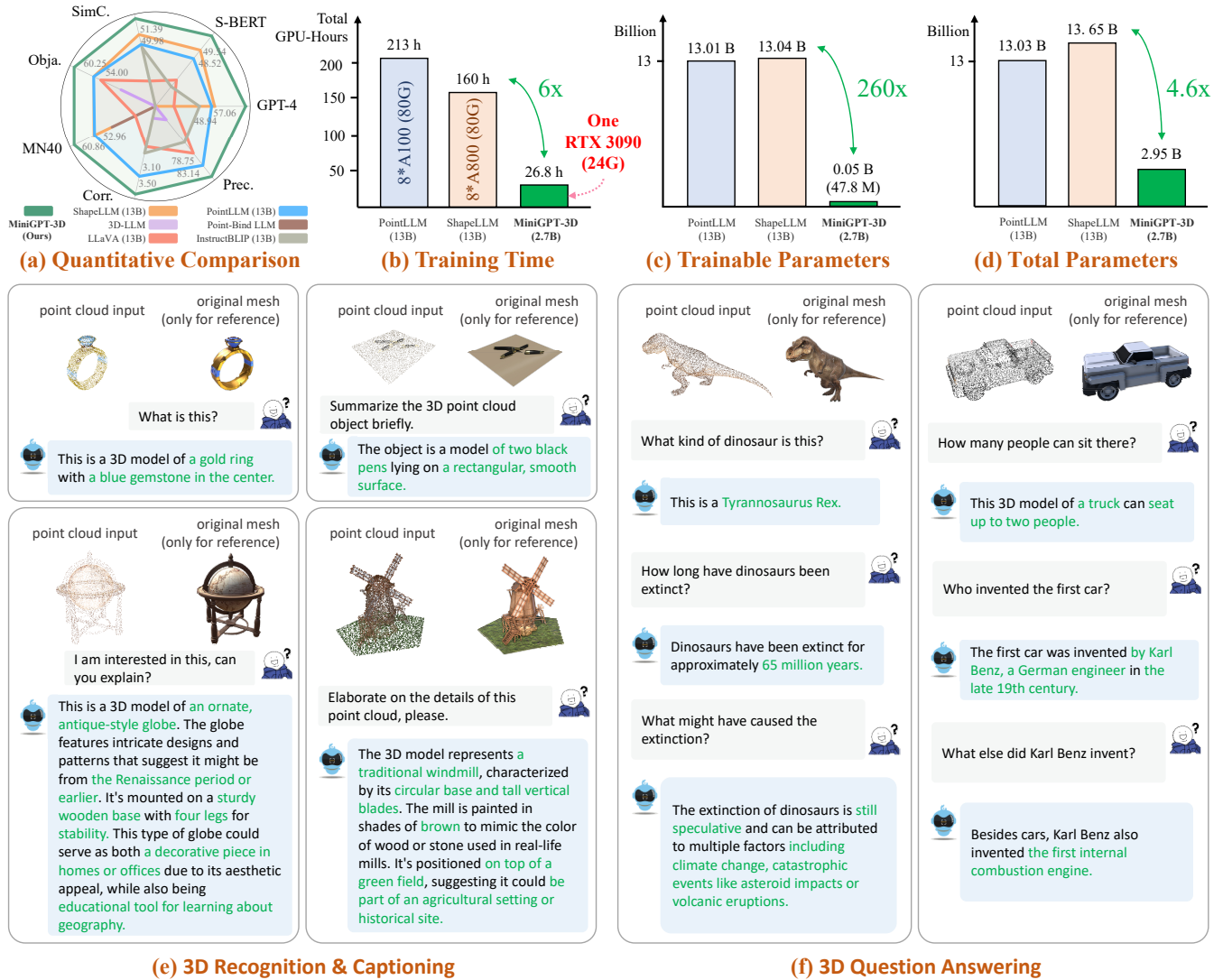


Figure 1: Demonstrations of MiniGPT-3D. We present MiniGPT-3D, an efficient and powerful 3D-LLM that aligns 3D point clouds with large language models using 2D priors from large 2D vision-language models. This figure demonstrates MiniGPT-3D’s superior performance and efficient training compared to existing 3D-LLMs. We also show some prediction examples in 3D recognition, captioning, and question-answering tasks, with the correct and fine-grained answers highlighted in green.

ABSTRACT

Large 2D vision-language models (2D-LLMs) have gained significant attention by bridging Large Language Models (LLMs) with images using a simple projector. Inspired by their success, large 3D point cloud-language models (3D-LLMs) also integrate point

clouds into LLMs. However, directly aligning point clouds with LLM requires expensive training costs, typically in hundreds of GPU-hours on A100, which hinders the development of 3D-LLMs. In this paper, we introduce **MiniGPT-3D**, an efficient and powerful 3D-LLM that achieves multiple SOTA results while training for only 27 hours on one RTX 3090. Specifically, we propose to

align 3D point clouds with LLMs using 2D priors from 2D-LLMs, which can leverage the similarity between 2D and 3D visual information. We introduce a novel four-stage training strategy for modality alignment in a cascaded way, and a mixture of query experts module to adaptively aggregate features with high efficiency. Moreover, we utilize parameter-efficient fine-tuning methods LoRA and Norm fine-tuning, resulting in only **47.8M** learnable parameters, which is up to 260× fewer than existing methods. Extensive experiments show that MiniGPT-3D achieves SOTA on 3D object classification and captioning tasks, with significantly cheaper training costs. Notably, MiniGPT-3D gains an 8.12 increase on GPT-4 evaluation score for the challenging object captioning task compared to ShapeLLM-13B, while the latter costs 160 total GPU-hours on 8 A800. We are the first to explore the efficient 3D-LLM, offering new insights to the community. Code and weights are available at <https://github.com/TangYuan96/MiniGPT-3D>.

CCS CONCEPTS

• **Computing methodologies** → **Computer vision; Natural language processing.**

KEYWORDS

Multimodal Large Language Models, Efficiently Multimedia Alignment, 3D Point Cloud Understanding

1 INTRODUCTION

Large Language Models (LLMs) have recently driven advancements in multiple fields [15, 35, 45, 46], benefiting from their world knowledge. Built on LLMs, large 2D vision-language models (2D-LLMs) [4, 27, 62] can align image features with text through an image feature projector, enabling 2D-LLMs to understand visual content. Inspired by 2D-LLMs, large 3D point cloud-language models (3D-LLMs) [39, 40, 51] aim to incorporate 3D point cloud features into LLMs, equipping LLMs with the ability to perceive and reason in 3D space. These 3D-LLMs hold promise for widespread applications in fields like robotics [44, 48] and autonomous driving [10, 15]. However, 3D-LLMs are expensive to train. For example, training PointLLM-13B [51] takes 213 total GPU-hours on 8 A100 GPU, making research and applications extremely challenging. Here, we aim to find a more efficient way to connect 3D point clouds with LLMs.

We observe that existing 3D-LLMs directly align point cloud encoders with LLMs. Although these encoders can produce somewhat unified features through multimodal pre-training, there is still a significant modality gap between 3D points with LLMs, requiring substantial resources for alignment. Besides, in contrast to resource-intensive alignment between vision and language, 3D point clouds and 2D images are both visual modalities, which makes it easier to align their representations. Thus, we pose a question: **Can we use 2D-LLMs as a strong prior to connect LLMs and 3D data, making alignment more efficient?** In other words, as shown in Figure 2, leveraging pre-trained 2D-LLMs directly allows for cutting down the cost of vision-language alignment, leaving only the 2D-3D vision alignment, which is significantly cheaper.

Following this intuition, we propose MiniGPT-3D, an efficient 3D-LLM that connects 3D point clouds and LLMs using 2D-LLMs as priors. Our MiniGPT-3D achieves multiple state-of-the-art (SOTA)

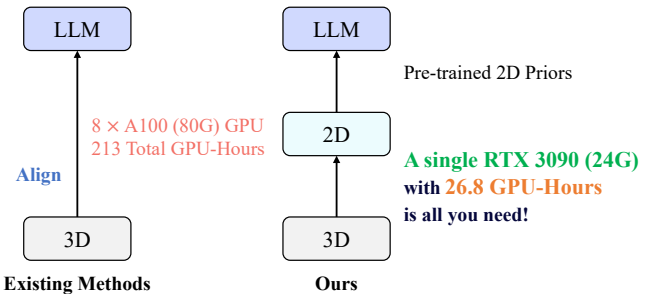


Figure 2: Existing methods and ours to align 3D with LLMs.

results, requiring only 27 hours of training on a single RTX 3090 GPU. Specifically, we propose an efficient four-stage training strategy in a cascaded way, gradually allowing the model to learn unified visual-textual representations. This process achieves the smooth transfer of priors from 2D-LLM to the 3D space, thus efficiently constructing a bridge from 3D to LLM. Moreover, we introduce the Mixture of Query Experts (MQE), which comprises multiple query experts and an expert router, enabling the adaptive aggregation of features from multiple experts with only 0.4M parameters. MQE dynamically adjusts the cooperation relationship between experts, thereby aggregating 3D features from multiple perspectives into the semantic space of 2D-LLM. Meanwhile, we employ various parameter-efficient fine-tuning (PEFT) technologies like LoRA [21] and Norm fine-tuning, and utilize an efficient LLM, further reducing the model’s training overhead.

As shown in Figure 1, MiniGPT-3D achieves new SOTA performance on generative 3D object classification and object captioning tasks. Specifically, compared to the powerful baseline ShapeLLM-13B [39], MiniGPT-3D achieves a 6.77% increase in classification average accuracy and an 8.12 increase in GPT-4 evaluation score. Notably, MiniGPT-3D utilizes extremely cheaper training resources (1× RTX 3090 vs. 8× A800), with up to 6× acceleration (26.8h on RTX 3090 vs. 160h on A800). Furthermore, our model has significantly fewer trainable parameters, reduced by up to 260×, with 2.95B model parameters in total, which is decreased by up to 4.6×.

MiniGPT-3D takes the first step in efficient 3D-LLM, we hope that MiniGPT-3D can bring new insights to this community. In summary, our contributions are as follows:

- We present MiniGPT-3D, an efficient and powerful 3D-LLM that aligns 3D points with LLMs using 2D priors, achieving multiple SOTA with only 26.8h of training on one RTX 3090.
- We propose an efficient four-stage training strategy in a cascaded way, gradually transferring the knowledge from 2D-LLMs to 3D while requiring only 47.8M learnable parameters.
- We design the mixture of query experts to aggregate multiple features from different experts with only 0.4M parameters.
- Extensive experiments show the superior performance of MiniGPT-3D on multiple tasks while reducing the training time and parameters by up to 6x and 260x, respectively.

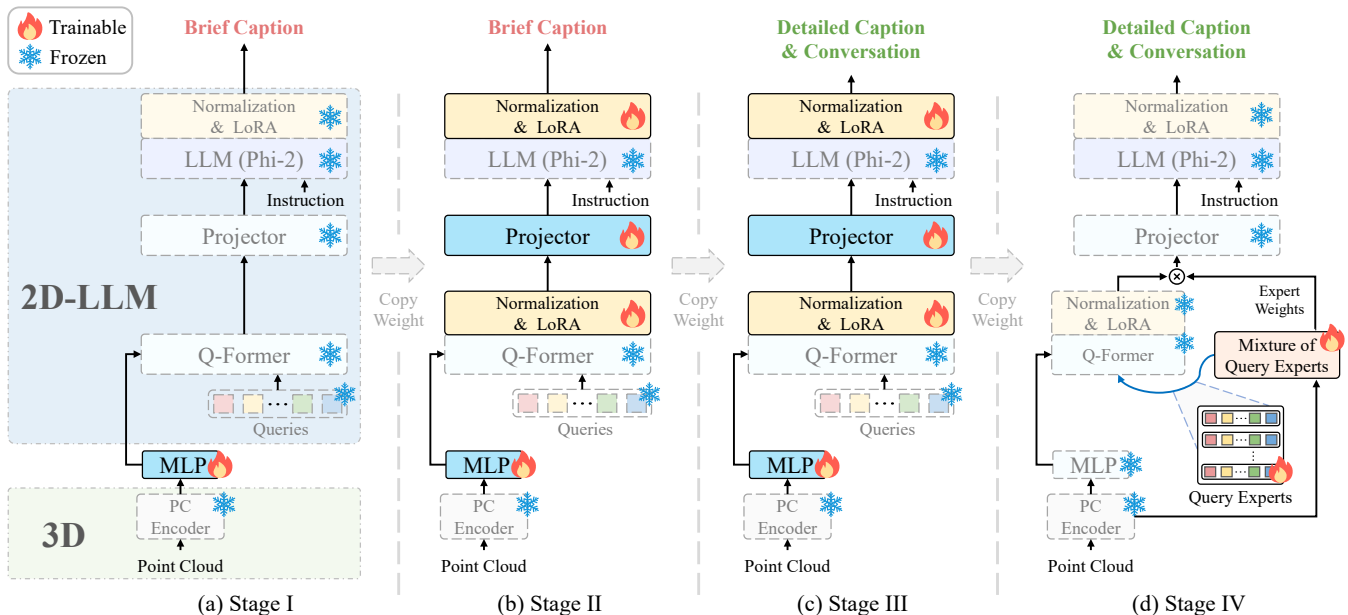


Figure 3: Training framework and strategy. Our MiniGPT-3D utilizes a four-stage training strategy. (a) We solely train the point cloud projection layer (MLP). (b) We train the modality projector while fine-tuning the point cloud projection layer, Q-Former, and LLM backbone. (c) We further enhance the modules trained in the second stage by leveraging a more challenging task. (d) Finally, we only train the mixture of query experts, while freezing the remaining modules.

2 RELATED WORK

2.1 Large 2D Vision-Language Models

The exceptional instruction-following and generalization capabilities of LLMs [46, 49, 53, 55] have been integrated into vision, leading to the emergence of large 2D vision-language models (2D-LLMs). Early works such as Flamingo [1] and BLP-2 [27] successfully use projectors to align vision information to LLMs. More recently, most works mainly focus on improving model capabilities through expanding the instruction-tuning dataset [5, 30, 61], increasing resolution of image [2, 31], enhancing image encoders [7, 59]. Meanwhile, some methods [8, 9, 57, 60] have also begun to explore efficient 2D-LLM. Models like TinyLlama [60] and TinyGPT-V [57] use Phi-2 [33], an efficient LLM, to achieve easily deployable 2D-LLMs. Among them, TinyGPT-V leverages LoRA [21] technology and pre-trained modules to achieve extremely efficient fine-tuning. However, TinyGPT-V can only handle 2D images, efficient 3D-LLM remains unexplored, and we aim to fill this gap.

2.2 Large 3D Point Cloud-Language Models

Large 3D point cloud-language models (3D-LLMs) introduce LLM into the point cloud modality [6, 20, 23, 29, 36, 39, 40, 51, 54]. Early attempt [20] renders 3D objects into 2D multi-view images, then utilizes 2D-LLM to understand 3D. However, the absence of direct perception of raw point cloud data limits its comprehension of 3D geometry. To address this issue, recent works [6, 23, 36, 40] propose to discard the “rendering” and encode point cloud directly, followed by modal alignment to fixed LLMs via trainable projectors. PointLLM [51] and ShapeLLM [39] show that models can be enhanced after fully fine-tuning. However, the training of 3D-LLMs

is expensive. For instance, PointLLM-13B requires training on 8 A100 GPUs for up to 216 total GPU-hours. We observe that with 2D-LLM as visual prior, we can not only bypass the “point cloud rendering”, but also make this hierarchical alignment extremely efficient. Therefore, we propose MiniGPT-3D, different from existing 3D-LLMs which aligns 3D points directly to LLMs, our MiniGPT-3D leverages the powerful priors from 2D-LLM as a linkage between LLM and 3D points, using only a RTX 3090 to train for 27 hours.

2.3 Mixture of Experts

Mixture of Experts (MoE) [22, 24] is an ensemble learning technique that adaptively activates selected modules, referred to as experts, based on input. MoE is widely used in various fields [14, 25, 26, 42, 43]. Shazeer et al. introduce MoE into NLP for the first time, where each intervening layer between LSTM layers serves as an expert. Gshard [26] further expands the MoE to Transformer [47], treating each Feed-Forward Neural Network (FFN) as an expert. Recently, with the emergence of LoRA, several works [13, 16, 58] design FFN’s LoRA network as an expert to efficiently fine-tune LLM. Moreover, OneLLM [19] introduces MoE to the learned projector of 2D-LLM, with each projector serving as an expert. In our work, we integrate the MoE concept into the queries of Q-Former [27], treating each set of queries as an expert. These experts adaptively aggregate point cloud features across diverse extraction perspectives.

3 METHOD

In this section, we first introduce the architecture of MiniGPT-3D (Sec. 3.1), and then present our four-stage training strategy (Sec. 3.2), and finally elucidate the training loss for MiniGPT-3D (Sec. 3.3).

3.1 Model Architecture

Figure 3 depicts the architecture of MiniGPT-3D, which consists of the six main components: a point cloud encoder, a point cloud projection layer (MLP), a Q-Former, a mixture of query expert (MQE), a modality projector, and a large language model.

The MiniGPT-3D framework introduces a two-step projection process, transforming the point cloud from 3D to 2D and then to 1D. Specifically, the point cloud is passed to the point cloud encoder to extract 3D features. Subsequently, features are then projected into a 2D semantic space using the point cloud projection layer. Finally, leveraging the 2D-LLM modules including the Q-Former, modality projector, Norm of LLM, and LoRA of LLM, features in 2D-LLM space are transduced into the 1D-text space of LLM, enabling efficient alignment between 3D and LLM. Additionally, MQE enhances MiniGPT-3D’s comprehensive and accurate perception of 3D objects. Details are presented in the following sections.

3.1.1 3D Features to 2D. During this process, the point cloud is encoded into 3D features and subsequently projected into the 2D semantic space of the 2D-LLM.

Point Cloud Encoder. The input point cloud is encoded into 3D features by the point cloud encoder f_{pc} . Specifically, the point cloud $P \in \mathbb{R}^{n \times d}$ is input to f_{pc} , where n is the number of points and d denotes the feature dimension of each point. Then, f_{pc} outputs a point feature sequence $X \in \mathbb{R}^{m \times b}$, comprising m features, each with a dimension of b . In our experiments, we employ the Point-BERT [56] model, pre-trained on ULIP-2 [52] using the Objaverse [12] dataset, as the point cloud encoder. To maintain pre-training knowledge, we freeze the encoder’s parameters on all training stages.

Point Cloud Projection Layer. The point cloud projection layer f_{MLP} is an MLP with two linear layers, which embeds point features X into the semantic space of the pre-trained 2D Q-Former [27], aligning their dimensions. Concisely, $Y = f_{MLP}(X)$, where $Y \in \mathbb{R}^{m \times b'}$ and b' is the hidden space dimension of Q-Former.

3.1.2 Features in 2D-LLM space to LLM. This part transduces the point cloud representation in the 2D semantic space of 2D-LLM to the 1D text space of LLM.

Q-Former. The Q-Former f_{QF} , with a decoder-based Transformer structure, transforms point features Y into point queries \bar{Q} . This process not only enhances the information extracted from point cloud features but also reduces input size for subsequent LLM, accelerating training and inference. Concisely, $\bar{Q} = f_{QF}(Y, Q)$, where $Q \in \mathbb{R}^{o \times b'}$, $\bar{Q} \in \mathbb{R}^{o \times b'}$. Q is the queries of Q-former and o is the number of query. In experiments, we initialize Q-Former with BLIP-2 [27] pre-trained weights. Given Q-Former’s extensive 105M parameters, we employ PEFT technologies to fine-tune its Query, Key, and Value layers, and normalization layers, thus enhancing adaptability to point clouds while preserving 2D knowledge.

Mixture of Query Experts. Inspired by multi-view image rendering for 3D-to-2D projection, we propose the Mixture of Query Experts (MQE) to achieve a similar effect. In the process of MQE, multiple sets of queries (query expert) are used to transform point features into the semantic space of 2D Q-Former. MQE is the first

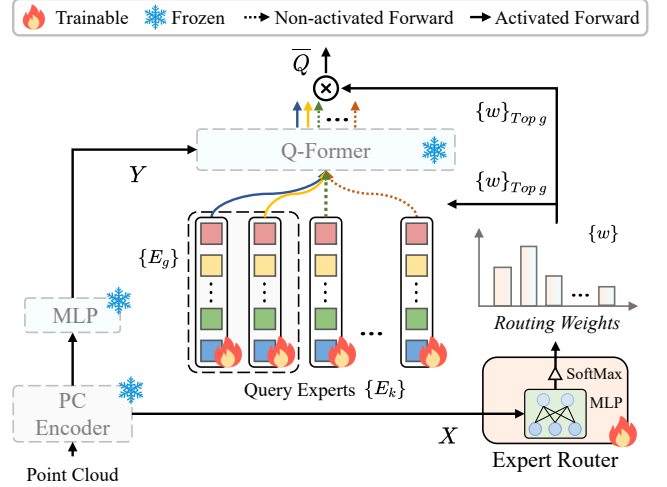


Figure 4: The framework of the mixture of query experts. First, a point cloud is encoded to features X and Y . Feature X is then passed through to the expert router, assigning softmax-based weights to experts. The top g experts are selected based on these weights. These experts, together with Y , are then fed into the Q-Former, and their outputs are weighted to produce the final point queries \bar{Q} .

to introduce dynamic routing of MoE into queries, enabling adaptive activation of more suitable query experts to capture richer semantic information across diverse point cloud inputs, as shown in Figure 4. MQE contains k trainable query experts $\{E_k\}$, each is a set of queries initialized from BLIP-2. To integrate multiple query experts into one set of queries, we use a dynamic routing, expert router f_R , which regulates each expert’s contribution. The expert router includes an MLP and a softmax operation, which accepts feature X and assigns softmax-based routing weights to each expert. We employ the sparse routing strategy [43], selecting g experts with the highest weights. Next, the selected query experts $\{E_g\}$ utilize Q-Former to extract high-dimensional semantics $\{Q_h\}$ from the feature Y . $\{Q_h\}$ are then weighted by the corresponding routing weights to generate the final point queries \bar{Q} . The process can be formulated as:

$$\bar{Q} = \sum_{E_q \in \{E_g\}} w_q \cdot f_{QF}(Y, E_q), \quad (1)$$

$$w_q = f_R(X) [q] = \text{Softmax}(\text{MLP}(X)) [q]. \quad (2)$$

To enable query experts to learn knowledge within a stable 3D-LLM semantic context, MQE is only utilized in the final training stage, by which time other modules have completed training.

Modality Projector. We use an MLP as the modality projector to bridge the modality gap between point cloud and text, while transforming point queries $\bar{Q} \in \mathbb{R}^{o \times b'}$ into point tokens $T_{pc} \in \mathbb{R}^{o \times c}$, where c denotes the shared dimension of both point and text tokens.

3.1.3 Large Language Model Backbone. To minimize GPU memory usage during training, we utilize Phi-2 [33] with 2.7 billion parameters as the large language model backbone of MiniGPT-3D.

Table 1: Each training stage setups and overhead.

Training Stages	Dataset Types	Dataset Scale	Epochs	Init_lr & Min_lr	Trainable Parameters	Training Time using One RTX 3090 GPU
Stage I	Brief Caption	660 k	1	3e-5, 1e-5	1.4 M	9.4 h
Stage II	Brief Caption	660 k	1	3e-5, 1e-5	47.4 M	10.9 h
Stage III	Detailed Caption & Conversation	70 k	3	1e-5, 1e-6	47.4 M	4.9 h
Stage IV	Detailed Caption & Conversation	70 k	1	5e-6, 1e-6	0.4 M	1.6 h

In MiniGPT-3D, the LLM backbone f_{llm} processes a sequence of tokens $T = (t_1, t_2, \dots, t_j) \in \mathbb{R}^{j \times c}$, where j is the number of tokens, including point tokens and text tokens. Leveraging the self-attention mechanism, the LLM backbone can comprehend the semantic relationships from different modality tokens and generate responses for given instructions. This process can be expressed as:

$$\hat{T} = f_{llm}(T), \quad (3)$$

where $\hat{T} = (\hat{t}_1, \hat{t}_2, \dots, \hat{t}_j) \in \mathbb{R}^{j \times c}$, and \hat{t}_i denotes the predicted i -th token, based on the semantics of all previous tokens $\{t_{<i}\}$. Subsequently, \hat{t}_i is passed through a linear layer $f_{llm \rightarrow vocab}$ to be mapped into the vocabulary space. A softmax operation is then applied to compute a probability distribution across the vocabulary, with the word of highest probability designated as the prediction z_i for \hat{t}_i . The process can be formulated as:

$$\tilde{t}_i = f_{llm \rightarrow vocab}(\hat{t}_i), \quad (4)$$

$$z_i = \arg \max_{w \in vocab} \text{Softmax}(\tilde{t}_i)[w]. \quad (5)$$

As LLMs are primarily trained on text, a perception gap arises when processing non-textual information. Therefore, we adapt PEFT technology LoRA [21] to the LLM backbone, and also further fine-tune the normalization layers, preserving learned knowledge and reducing computational overhead.

3.2 Training Stages

To gradually transfer the priors of 2D-LLM to point cloud modality and enhance the nascent 3D-LLM’s comprehension, our training process includes four stages, each focusing on a distinct task, as shown in Figure 3. The following subsections will describe them.

3.2.1 Stage I. As shown in Figure 3(a), the first stage aims to bridge the knowledge gap between the 3D point cloud encoder and 2D-LLM modules, facilitating a seamless transition from 3D to 2D. We solely train the point cloud projection layer (MLP), with other modules frozen. Initialization is sourced from ULIP-2 [52] for the encoder, BLIP-2 [27] for Q-Former, and TinyGPT-V [57] for normalization layers of LLM, LoRA of LLM, and the modality projector. Since the frozen Q-Former from BLIP-2 is also used in TinyGPT-V, MiniGPT-3D only owns two knowledge domains from 3D of ULIP-2 and 2D-LLM of TinyGPT-V before training. To build a robust bridge between domains, we train the projection layer using 660k caption-point cloud pairs, involving 1.4M parameters, as detailed in Table 1.

3.2.2 Stage II. In the second stage, our objective is to transfer the vision-language knowledge domain to 3D space, establishing the 3D-language knowledge domain. As shown in Figure 3(b), we fine-tune four parts: the point cloud projection layer (MLP), the Q-Former, the modality projector, and the LLM. Utilizing the 3D-2D bridge of the

first stage, 2D-LLM modules, via fine-tuning, gain comprehension of 3D point clouds and gradually transfer the powerful priors to be the 3D-language knowledge. During this process, to minimize the impact of the 3D-2D bridge, we employ the identical dataset from the first stage to train 47.4M parameters, as outlined in Table 1.

3.2.3 Stage III. To gain better 3D-language knowledge, we further fine-tune the modules trained in the second stage and utilize a more challenging dataset, including detailed caption-point cloud pairs and conversations, to empower MiniGPT-3D with the capabilities to comprehend and respond to complex instructions.

3.2.4 Stage IV. During the prior stages, using a single set of queries restricts 3D perception perspective, leading to incomplete cognition. To refine MiniGPT-3D’s perception, we introduce MQE to adaptively activate suitable multiple query experts for Q-Former, as shown in Figure 3(d). Distinct from the preceding three stages focusing on rapidly establishing 3D-language knowledge, this stage presents a stable semantic context for query experts to learn knowledge efficiently. Specifically, we only fine-tune 0.4M MQE-related parameters, reusing the dataset from the third stage to minimize the impact of data distribution changes, as outlined in Table 1.

3.3 Training Objective

The training objective of MiniGPT-3D aims to minimize the discrepancy between predicted and true probability distributions at each token position. Given a point cloud and corresponding text instruction, MiniGPT-3D outputs a sequence \hat{T} . Next, \hat{T} is processed by $f_{llm \rightarrow vocab}$ and then a softmax operation is applied to obtain the probability distribution over the vocabulary for each output token, denoted as \bar{T} . The training loss is formulated as follows:

$$\mathcal{L} = \text{CrossEntropy}(h(G), \bar{T}), \quad (6)$$

where the $h(\cdot)$ represents the LLM’s tokenizer. G is the ground truth text. The $\text{CrossEntropy}(\cdot)$ refers to the cross-entropy loss function. Notably, we only compute the loss for the generated text.

4 EXPERIMENTS

4.1 Experimental Settings

Utilizing one RTX 3090 GPU with 24GB of RAM, we train MiniGPT-3D with only 47.8M trainable parameters in 26.8 hours. We adopt the AdamW optimizer with a weight decay of 0.05 and a cosine decay with linear warm up learning rate schedule. The initial learning rate decreases gradually as the training stage advances, as shown in Table 1. We use the point-text instruction dataset [51], including 660K brief-description instructions and 70K complex instructions. 200 objects are split as test data, following PointLLM [51] and ShapeLLM [39]. For each input point cloud $P \in \mathbb{R}^{n \times d}$, the number of point n is 8192, and the dimension d is 6. We default point clouds

Table 2: Generative 3D object classification results on the ModelNet40 test split and Objaverse. The accuracy (%) under the Instruction-typed (I) prompt “What is this?” and the Completion-type (C) prompt “This is an object of” are reported. The bold and underline indicate the best and second best results, respectively.

Model	Reference	LLM Size	Trainable Params	Input	ModelNet40			Objaverse			Average
					(I)	(C)	Average	(I)	(C)	Average	
InstructBLIP-7B [11]	NeurIPS,23	7B	0.20B	Single-V. Img.	19.53	31.48	25.51	45.00	42.00	43.50	34.50
InstructBLIP-13B [11]	NeurIPS,23	13B	0.20B	Single-V. Img.	25.97	31.40	28.69	37.00	31.50	34.25	31.47
LLaVA-7B [32]	NeurIPS,23	7B	7.03B	Single-V. Img.	39.75	39.67	39.71	49.50	50.50	50.00	44.86
LLaVA-13B [32]	NeurIPS,23	13B	13.03B	Single-V. Img.	37.12	36.06	36.59	53.00	50.50	51.75	44.17
3D-LLM [20]	NeurIPS,23	13B	-	3D Obj. + Mul.-V. Img.	-	-	-	49.00	41.50	45.25	45.25
Point-Bind LLM [18]	arXiv,23.9	7B	-	3D Point Cloud	51.90	39.71	45.81	6.00	4.50	5.25	25.53
PointLLM-7B [51]	arXiv,23.8	7B	7.01B	3D Point Cloud	<u>53.44</u>	51.82	52.63	55.00	51.00	53.00	52.82
PointLLM-13B [51]	arXiv,23.8	13B	13.01B	3D Point Cloud	<u>53.00</u>	<u>52.55</u>	52.78	<u>56.50</u>	<u>51.50</u>	54.00	53.39
ShapeLLM-7B [39]	arXiv,24.2	7B	7.04B	3D Point Cloud	-	-	<u>53.08</u>	-	-	<u>54.50</u>	53.79
ShapeLLM-13B [39]	arXiv,24.2	13B	13.04B	3D Point Cloud	-	-	52.96	-	-	54.00	53.48
MiniGPT-3D	-	2.7B	0.05B (47.8M)	3D Point Cloud	61.75 (+8.31)	59.97 (+7.42)	60.86 (+7.78)	60.00 (+3.5)	60.50 (+9.00)	60.25 (+5.75)	60.56 (+6.77)

Table 3: 3D object captioning results on Objaverse. The results are from human evaluation, GPT-4 evaluation, and traditional metrics. The bold and underline indicate the best and second best results, respectively.

Model	Reference	LLM Size	Trainable Params	GPT-4	Sentence-BERT	SimCSE	Human Evaluation		
							Correctness	Hallucination ↓	Precision
InstructBLIP-7B [11]	NeurIPS,23	7B	0.20B	45.34	47.41	48.48	2.56	0.77	76.99
InstructBLIP-13B [11]	NeurIPS,23	13B	0.20B	44.97	45.90	48.86	2.58	1.13	69.56
LLaVA-7B [32]	NeurIPS,23	7B	7.03B	46.71	45.61	47.10	2.76	0.86	76.30
LLaVA-13B [32]	NeurIPS,23	13B	13.03B	38.28	46.37	45.90	2.43	0.86	73.97
3D-LLM [20]	NeurIPS,23	13B	-	33.42	44.48	43.68	1.77	1.16	60.39
PointLLM-7B [51]	arXiv,23.8	7B	7.01B	44.85	47.47	48.55	3.04	0.66	<u>82.14</u>
PointLLM-13B [51]	arXiv,23.8	13B	13.01B	48.15	47.91	49.12	<u>3.10</u>	0.84	<u>78.75</u>
ShapeLLM-7B [39]	arXiv,24.2	7B	7.04B	46.92	48.20	49.23	-	-	-
ShapeLLM-13B [39]	arXiv,24.2	13B	13.04B	48.94	<u>48.52</u>	49.98	-	-	-
MiniGPT-3D	-	2.7B	0.05B (47.8M)	57.06 (+8.12)	49.54 (+1.02)	51.39 (+1.41)	3.50 (+0.40)	0.71 (+0.05)	83.14 (+1.00)

without color to black. For a fair comparison, we adopt the identical versions models of GPT-4 [35] (“gpt-4-0613”) and ChatGPT [34] (“gpt-3.5-turbo-0613”) as our evaluation tools, like prior works [39, 51]. We choose multiple SOTA 3D-LLMs [18, 20, 39, 51] and two popular open-source 2D-LLMs [11, 32] as our baselines.

4.2 Generative 3D Object Classification

We conduct the generative 3D object classification tasks [51] on ModelNet40 [50] and Objaverse [12] datasets to assess MiniGPT-3D’s categorical cognitive ability.

Settings. For a fair comparison, we utilize the classification evaluation settings similar to prior works [39, 51]. We employ identical prompts: the Instruction-typed (I) prompt “What is this?” and the Completion-type (C) prompt “This is an object of”. Point clouds and these prompts are fed into our MiniGPT-3D, outputting textual responses. For close-set zero-shot classification on ModelNet40, ChatGPT processes the text responses of MiniGPT-3D to select predicted categories from 40 ModelNet40 classes. For open-vocabulary classification on Objaverse, GPT-4 is employed as an evaluator to determine whether MiniGPT-3D’s text response refers to the same category as the ground-truth caption.

Results. Experimental results are shown in Table 2. We achieve SOTA performance on all classification benchmarks using only one

RTX 3090. Specifically, compared to the best baseline, ShapeLLM [39], we achieve significant improvements of 7.78% and 5.75% in average accuracy on ModelNet40 and Objaverse datasets, respectively. Unlike other methods using LLM (7B or 13B) that require fine-tuning on 8 A100 or 8 A800 for hundreds of total GPU-hours, our MiniGPT-3D only utilizes a 2.7B LLM and trains 47.8M parameters on a single RTX 3090 GPU in 27 hours. These demonstrate the superiority and efficiency of our MiniGPT-3D, which leverages the powerful priors from 2D-LLMs to build 3D-LLM. Additionally, we observe that MiniGPT-3D exhibits the best performance in recognizing 3D objects of the ModelNet40 dataset unused during training, indicating its stronger generalization ability compared to other methods. Furthermore, even if using different prompts (I and C) on the Objaverse dataset, MiniGPT-3D demonstrates highly consistent classification performance compared to other 3D-LLMs that have a 4% accuracy gap, showcasing its robustness for diverse prompts.

4.3 3D Object Captioning

To assess the model’s understanding of 3D object details, we perform the 3D object captioning task.

Settings. For a fair comparison, we follow the evaluation settings of prior works [39, 51]. We use the prompt “Caption this 3D model in detail”. We adopt three distinct evaluation methods: human evaluation, GPT-4 [35] evaluation, and traditional metric evaluation. In

Table 4: Qualitative comparisons. The classification and caption results of models on ModelNet40 and Objaverse are presented. Our MiniGPT-3D generates more detailed and insightful responses compared to other baselines.

Samples 1, 2		
Prompt	What is this?	Briefly caption this 3D model.
Ground Truth	Laptop	A cartoon black monster like a dragon
InstructBLIP-13B [11]	symbol letter l	a black lizard with a sharp tooth in a dark room
LLaVA-13B[32]	A small, grainy, black and white letter j.	A 3D model of a dark, menacing dragon.
3D-LLM [20]	-	A black and white tiger with long legs, standing on its hind leg.
Point-Bind LLM [18]	This is a laptop computer.	The 3D model features a large, ornate gargoyle with a horned helmet, sitting on top of a building.
PointLLM-13B [51]	The 3D model represents a notebook computer, typically a laptop.	The 3D model depicts a menacing black dragon, with its mouth opened wide revealing a row of sharp teeth.
MiniGPT-3D	This is a 3D model of a sleek, black laptop. The laptop is rectangular in shape and has a glossy finish, suggesting a high-quality build. It has a flat screen, which is a common feature in modern laptops, and it's equipped with a keyboard and a touchpad for user interaction. The laptop appears to be in good condition, suggesting it could be used for various tasks such as work, entertainment, or education.	This is a 3D model of a fearsome, black-colored dinosaur. The dinosaur possesses an aggressive stance, with sharp claws extending from its arms and legs. It has long black fangs that seem ready to attack.

Table 5: Ablation on training process.

Row No.	Stage I	Stage II	Stage III	Stage IV	Acc.
1	✓				39.10
2	✓	✓			55.92
3	✓	✓	✓		59.10
4	✓	✓	✓	✓	60.56
5	✓		✓	✓	52.81
6		✓	✓	✓	58.46
7	✓	✓		✓	47.93

Table 6: Ablation on 2D priors from 2D-LLM.

Modality Projector	Norm and LoRA for LLM	Acc.
		49.04
✓		57.44
	✓	57.86
✓	✓	58.46

Table 7: Ablation on stages using MQE.

Stage I	Stage II	Stage III	Stage IV	Acc.
✓				58.83
	✓			60.25
		✓		59.50
			✓	60.56

human evaluation, volunteers evaluate the model using standardized processes from PointLLM [51]. Specifically, focusing on object attributes (such as type, color, material, etc.), volunteers visually assess objects and assign correctness scores and hallucination scores to captions. Correctness measures model accuracy in describing attributes, while hallucination evaluates fabricated details' severity. Each attribute, correct or hallucinated, receives a point. Precision is calculated as the ratio of correct information in model-generated content. The Inter-Annotator Agreement score is 0.89 on ICC1k, indicating volunteers' high consistency in cognitive understanding and scoring criteria. GPT-4 evaluates semantic similarity between our model's output and manually annotated captions. In traditional metric evaluation, like prior works [39, 51], we use data-driven metrics like Sentence-BERT [41] and SimCSE [17], instead of BLEU-1 [37], ROUGE [28], and METEOR [3], because the latter lack sufficient capabilities in semantic evaluation.

Results. As shown in Table 3, our MiniGPT-3D achieves SOTA performance on multiple metrics. Specifically, MiniGPT-3D outperforms ShapeLLM-13B [39], by a large margin of 8.12 on the GPT-4 evaluation score, setting new SOTA with only 2.7B LLM, indicating robust 3D detail comprehension. Also, compared to ShapeLLM-13B, MiniGPT-3D surpasses 1.02 and 1.41 on Sentence-BERT and SimCSE metrics, respectively, achieving new SOTA with its remarkable ability to generate accurate captions matching ground truth. Human evaluation further reveals MiniGPT-3D's superior correctness and precision scores compared to baselines. Notably, even with a 2.7B LLM, MiniGPT-3D exhibits a hallucination score comparable to

SOTA, surpassing larger 13B LLM-based methods. These outstanding results showcase MiniGPT-3D's fine-grained understanding of 3D objects, inheriting the cognitive capabilities of 2D-LLM.

4.4 Qualitative Results

Figure 1(e) qualitatively shows the MiniGPT-3D's powerful ability to perceive 3D object details. Our MiniGPT-3D precisely extracts information from 3D objects, encompassing categories, colors, shapes, materials, and internal component relationships. Additionally, MiniGPT-3D can perform reasonable reasoning based on object cues, such as potential occurrence periods and locations. Figure 1(f) further demonstrates MiniGPT-3D's comprehension of 3D object information in open-ended dialogues. MiniGPT-3D accurately outputs 3D object-related world knowledge, showcasing its extensive textual knowledge inherited from LLMs.

In sample 1 of Figure 4, our MiniGPT-3D successfully recognizes the shape, screen, and keyboard of a laptop, compared to other methods. Furthermore, it can deduce the potential usage of this 3D object. In the more complex sample 2 of Figure 4, our MiniGPT-3D demonstrates superior understanding capabilities of 3D objects by recognizing additional features like the dinosaur's sharp claws and inferring its potential action intentions, compared to other methods.

4.5 Ablation Studies

In this section, we conduct ablation studies to investigate various model design options. Herein, we report the total average accuracy of MiniGPT-3D on the generative classification benchmark.

Table 8: Ablation on fine-tuned modules in Q-Former.

LoRA Q, K, V	LoRA Dense	Norm	Acc.
			58.18
✓			59.85
✓	✓		59.97
✓	✓	✓	60.14
✓		✓	60.56

Table 10: Ablation on the point cloud projection layers.

Number of layers	Acc.
1	57.02
2	60.56
3	59.20

Table 12: Ablation on trained modules in stage IV.

MQE	Norm. & LoRA for Q-Former	Modality Projector	Norm. & LoRA for LLM	MLP	Acc.
✓	✓	✓	✓	✓	58.93
✓	✓	✓	✓		59.93
✓	✓	✓			59.02
✓	✓				59.64
✓					60.56

4.5.1 Training process. We conduct ablation study to validate the efficacy of our four-stage training strategy. The results in Table 5 highlight the optimal performance achieved by our approach. Specifically, comparing Row #4 vs. #6, we observe that the first stage bridges knowledge between 2D-LLM and 3D encoder, enabling smoother semantic transitions across different dimensional spaces. Comparing Row #4 vs. #5, we note that the second training stage which involves using easy tasks to adapt the knowledge of the 2D-LLM to the 3D space, allows the model to focus on enhancing cognitive capabilities in subsequent stages. Comparing Row #4 vs. #7, the third training stage utilizes more challenging tasks to reinforce the newborn 3D cognitive abilities, providing a reliable semantic context for the final stage to train MQE. Comparing Row #4 vs. #3, the inclusion of the fourth stage, dedicated to training the MQE, enables each query expert to acquire unique knowledge, further enhancing MiniGPT-3D’s understanding of 3D objects.

4.5.2 2D priors from 2D-LLM. We conduct ablation study to verify the effectiveness of the 2D priors from 2D-LLM, as detailed in Table 6. Since dropping any pre-trained weights of 2D-LLM would make the first training stage infeasible, all cases of this ablation study are just trained through stages II to IV. We find that removing any of 2D-LLM weight degrades performance, and discarding more pre-trained weights of 2D-LLM causes an up to 9.4% accuracy drop. These results highlight the crucial role of 2D-LLM knowledge in boosting 3D-LLM performance. Using 2D-LLM modules facilitates cost-efficient training of 3D-LLM even on consumer GPUs like RTX 3090 GPU, enhancing accessibility for the community.

4.5.3 Training stages using MQE. We further investigate the impact of training MQE in different stages, with detailed results presented in Table 7. Our results indicate that introducing MQE in only stage IV achieves optimal performance. The I-III stages enable

Table 9: Ablation on the number of query experts.

Number	Acc.
1	59.19
3	59.66
6	59.14
8	60.56
10	59.85

Table 11: Ablation on router type of MQE.

Type	Acc.
Constant Router	60.10
Sparse Router	60.56
Soft Router	60.31

the model to learn enough semantic features, paving the way for MQE to adaptively select useful information in stage IV.

4.5.4 Fine-tuned modules in Q-Former. Employing PEFT methods to fine-tune Q-Former can better align point features with LLM, avoiding expensive computation. As outlined in Table 8, fine-tuning the Query, Key, and Value layers with LoRA [21], along with normalization layers, maximizes the potential of Q-Former. Notably, we efficiently fine-tune the 105M-parameter Q-Former using only 0.7M parameters, achieving a 2.38% accuracy improvement compared to the frozen Q-Former.

4.5.5 Number of query experts. Within MQE, each query expert holds unique knowledge, facilitating extraction of point cloud features. Our experiments in Table 9, reveal that 8 query experts yield optimal performance. Insufficient experts may compromise information extraction, while excessive ones may affect cooperation among experts. Notably, single-expert, i.e. without MQE, results in a 1.37% accuracy drop, highlighting the superiority of MQE.

4.5.6 Point cloud projection layer. The point cloud projection layer bridges point cloud features with the 2D semantics of frozen Q-Former, while ensuring dimensional alignment. As shown in Table 10, our experiments demonstrate that two MLP layers offer the optimal setup, as excessive or insufficient layers can result in information loss, compromising overall performance.

4.5.7 Router type of MQE. The routing mechanism in MQE regulates the cooperation among query experts. The constant router [25] assigns static average weights, while the soft router [38] dynamically assigns weights during training. The sparse router [43] selects the top two experts based on the dynamic weights provided by the soft router. We explore these router types in Table 11, finding that the sparse router, which dynamically assigns weights and selects the most promising experts, maximizes the capabilities of MQE.

4.5.8 Trained modules in stage IV. In the training stage IV, only MQE is trained to enable each query expert to learn knowledge within a stable semantic context. Our experiments in Table 12 investigate the integration of various training modules. The results indicate that stage IV is to adaptively aggregate features of different experts, with knowledge gained from I-III stages frozen. Losing any frozen knowledge causes information loss, demonstrating the MQE is specifically designed for information aggregation.

5 CONCLUSION

In this paper, we present MiniGPT-3D, a efficient and powerful 3D-LLM, requiring the training of only 47.8M learnable parameters within 26.8 hours on one single NVIDIA RTX 3090 GPU. Specifically, we propose a novel four-stage training strategy that gradually aligns 3D point cloud features with LLM using 2D priors from 2D-LLM. Additionally, we design the mixture of query experts, introducing MoE to queries, to adaptively aggregate multiple features. Extensive experiments show the superiority of MiniGPT-3D in 3D point cloud understanding and question answering.

Discussion. MiniGPT-3D’s limitations lie in its training on object-level datasets, preventing it from understanding large-scale point clouds. Moreover, like existing 3D-LLMs, our MiniGPT-3D

solely focuses on comprehending static 3D objects, lacking the capacity to recognize the actions of dynamic objects. We will extend our 3D-LLM building approach to autonomous driving scenarios.

REFERENCES

- [1] Jean-Baptiste Alayrac, Jeff Donahue, Pauline Luc, Antoine Miech, Iain Barr, Yana Hasson, Karel Lenc, Arthur Mensch, Katherine Millican, Malcolm Reynolds, et al. 2022. Flamingo: a visual language model for few-shot learning. *Advances in neural information processing systems* 35 (2022), 23716–23736.
- [2] Jinze Bai, Shuai Bai, Shusheng Yang, Shijie Wang, Sinan Tan, Peng Wang, Junyang Lin, Chang Zhou, and Jingren Zhou. 2023. Qwen-vl: A frontier large vision-language model with versatile abilities. *arXiv preprint arXiv:2308.12966* (2023).
- [3] Satantjeev Banerjee and Alon Lavie. 2005. METEOR: An automatic metric for MT evaluation with improved correlation with human judgments. In *Proceedings of the acl workshop on intrinsic and extrinsic evaluation measures for machine translation and/or summarization*. 65–72.
- [4] Junbum Cha, Wooyoung Kang, Jonghwan Mun, and Byungseok Roh. 2023. Honeybee: Locality-enhanced projector for multimodal llm. *arXiv preprint arXiv:2312.06742* (2023).
- [5] Lin Chen, Jisong Li, Xiaoyi Dong, Pan Zhang, Conghui He, Jiaqi Wang, Feng Zhao, and Dahua Lin. 2023. Sharegpt4v: Improving large multi-modal models with better captions. *arXiv preprint arXiv:2311.12793* (2023).
- [6] Sijin Chen, Xin Chen, Chi Zhang, Mingsheng Li, Gang Yu, Hao Fei, Hongyuan Zhu, Jiayuan Fan, and Tao Chen. 2023. LL3DA: Visual Interactive Instruction Tuning for Omni-3D Understanding, Reasoning, and Planning. *arXiv preprint arXiv:2311.18651* (2023).
- [7] Zhe Chen, Jiannan Wu, Wenhai Wang, Weijie Su, Guo Chen, Sen Xing, Zhong Muyan, Qinglong Zhang, Xizhou Zhu, Lewei Lu, et al. 2023. Internvl: Scaling up vision foundation models and aligning for generic visual-linguistic tasks. *arXiv preprint arXiv:2312.14238* (2023).
- [8] Xiangxiang Chu, Limeng Qiao, Xinyang Lin, Shuang Xu, Yang Yang, Yiming Hu, Fei Wei, Xinyu Zhang, Bo Zhang, Xiaolin Wei, et al. 2023. Mobilevlm: A fast, reproducible and strong vision language assistant for mobile devices. *arXiv preprint arXiv:2312.16886* (2023).
- [9] Xiangxiang Chu, Limeng Qiao, Xinyu Zhang, Shuang Xu, Fei Wei, Yang Yang, Xiaofei Sun, Yiming Hu, Xinyang Lin, Bo Zhang, et al. 2024. MobileVLM V2: Faster and Stronger Baseline for Vision Language Model. *arXiv preprint arXiv:2402.03766* (2024).
- [10] Can Cui, Yunsheng Ma, Xu Cao, Wenqian Ye, and Ziran Wang. 2024. Drive as you speak: Enabling human-like interaction with large language models in autonomous vehicles. In *Proceedings of the IEEE/CVF Winter Conference on Applications of Computer Vision*. 902–909.
- [11] Wenliang Dai, Junnan Li, Dongxu Li, Anthony Meng Huat Tiong, Junqi Zhao, Weisheng Wang, Boyang Li, Pascale N Fung, and Steven Hoi. 2024. Instruct-blip: Towards general-purpose vision-language models with instruction tuning. *Advances in Neural Information Processing Systems* 36 (2024).
- [12] Matt Deitke, Dustin Schwenk, Jordi Salvador, Luca Weihs, Oscar Michel, Eli VanderBilt, Ludwig Schmidt, Kiana Ehsani, Anirudha Kembhavi, and Ali Farhadi. 2023. Objaverse: A universe of annotated 3d objects. In *Proceedings of the IEEE/CVF Conference on Computer Vision and Pattern Recognition*. 13142–13153.
- [13] Shihan Dou, Enyu Zhou, Yan Liu, Songyang Gao, Jun Zhao, Wei Shen, Yuhao Zhou, Zhiheng Xi, Xiao Wang, Xiaoran Fan, et al. 2023. Lora-moe: Revolutionizing mixture of experts for maintaining world knowledge in language model alignment. *arXiv preprint arXiv:2312.09979* (2023).
- [14] William Fedus, Barret Zoph, and Noam Shazeer. 2022. Switch transformers: Scaling to trillion parameter models with simple and efficient sparsity. *Journal of Machine Learning Research* 23, 120 (2022), 1–39.
- [15] Daocheng Fu, Xin Li, Licheng Wen, Min Dou, Pinlong Cai, Botian Shi, and Yu Qiao. 2024. Drive like a human: Rethinking autonomous driving with large language models. In *Proceedings of the IEEE/CVF Winter Conference on Applications of Computer Vision*. 910–919.
- [16] Chongyang Gao, Kezhen Chen, Jimeng Rao, Baochen Sun, Ruibo Liu, Daiyi Peng, Yawen Zhang, Xiaoyuan Guo, Jie Yang, and VS Subrahmanian. 2024. Higher Layers Need More LoRA Experts. *arXiv preprint arXiv:2402.08562* (2024).
- [17] Tianyu Gao, Xingcheng Yao, and Danqi Chen. 2021. Simcse: Simple contrastive learning of sentence embeddings. *arXiv preprint arXiv:2104.08821* (2021).
- [18] Ziyu Guo, Renrui Zhang, Xiangyang Zhu, Yiwen Tang, Xianzheng Ma, Jiaming Han, Kexin Chen, Peng Gao, Xianzhi Li, Hongsheng Li, et al. 2023. Point-bind & point-llm: Aligning point cloud with multi-modality for 3d understanding, generation, and instruction following. *arXiv preprint arXiv:2309.00615* (2023).
- [19] Jiaming Han, Kaixiong Gong, Yiyuan Zhang, Jiaqi Wang, Kaipeng Zhang, Dahua Lin, Yu Qiao, Peng Gao, and Xiangyu Yue. 2023. Onellm: One framework to align all modalities with language. *arXiv preprint arXiv:2312.03700* (2023).
- [20] Yining Hong, Haoyu Zhen, Peihao Chen, Shuhong Zheng, Yilun Du, Zhenfang Chen, and Chuang Gan. 2024. 3d-llm: Injecting the 3d world into large language models. *Advances in Neural Information Processing Systems* 36 (2024).
- [21] Edward J Hu, Yelong Shen, Phillip Wallis, Zeyuan Allen-Zhu, Yuanzhi Li, Shean Wang, Lu Wang, and Weizhu Chen. 2021. Lora: Low-rank adaptation of large language models. *arXiv preprint arXiv:2106.09685* (2021).
- [22] Robert A Jacobs, Michael I Jordan, Steven J Nowlan, and Geoffrey E Hinton. 1991. Adaptive mixtures of local experts. *Neural computation* 3, 1 (1991), 79–87.
- [23] Jiayi Ji, Haowei Wang, Changli Wu, Yiwei Ma, Xiaoshuai Sun, and Rongrong Ji. 2023. JM3D & JM3D-LLM: Elevating 3D Representation with Joint Multi-modal Cues. *arXiv preprint arXiv:2310.09503* (2023).
- [24] Michael I Jordan and Robert A Jacobs. 1994. Hierarchical mixtures of experts and the EM algorithm. *Neural computation* 6, 2 (1994), 181–214.
- [25] Sneha Kudugunta, Yanping Huang, Ankur Bapna, Maxim Krikun, Dmitry Lepikhin, Minh-Thang Luong, and Orhan Firat. 2021. Beyond distillation: Task-level mixture-of-experts for efficient inference. *arXiv preprint arXiv:2110.03742* (2021).
- [26] Dmitry Lepikhin, Hyoukjoong Lee, Yuanzhong Xu, Dehao Chen, Orhan Firat, Yanping Huang, Maxim Krikun, Noam Shazeer, and Zhifeng Chen. 2020. Gshard: Scaling giant models with conditional computation and automatic sharding. *arXiv preprint arXiv:2006.16668* (2020).
- [27] Junnan Li, Dongxu Li, Silvio Savarese, and Steven Hoi. 2023. Blip-2: Bootstrapping language-image pre-training with frozen image encoders and large language models. In *International conference on machine learning*. PMLR, 19730–19742.
- [28] Chin-Yew Lin. 2004. Rouge: A package for automatic evaluation of summaries. In *Text summarization branches out*. 74–81.
- [29] Dingning Liu, Xiaoshui Huang, Yuenan Hou, Zhihui Wang, Zhenfei Yin, Yongshun Gong, Peng Gao, and Wanli Ouyang. 2024. Uni3D-LLM: Unifying Point Cloud Perception, Generation and Editing with Large Language Models. *arXiv preprint arXiv:2402.03327* (2024).
- [30] Fuxiao Liu, Kevin Lin, Linjie Li, Jianfeng Wang, Yaser Yacoub, and Lijuan Wang. 2023. Aligning large multi-modal model with robust instruction tuning. *arXiv preprint arXiv:2306.14565* (2023).
- [31] Haotian Liu, Chunyuan Li, Yuheng Li, and Yong Jae Lee. 2023. Improved baselines with visual instruction tuning. *arXiv preprint arXiv:2310.03744* (2023).
- [32] Haotian Liu, Chunyuan Li, Qingyang Wu, and Yong Jae Lee. 2024. Visual instruction tuning. *Advances in neural information processing systems* 36 (2024).
- [33] Abdin Marah, Aneja Jyoti, Bubeck Sebastien, César Teodoro Mendes Caio, Chen Weizhu, Del Giorno Allie, Eldan Ronen, Gopi Sivakanth, Gunasekar Suriya, Javarheripi Mojan, Kauffmann Piero, Tat Lee Yin, Li Yuanzhi, Nguyen Anh, de Rosa Gustavo, Saarikivi Olli, Salim Adil, Shah Shital, Santacroce Michael, Singh Behl Harkirat, Taumann Kalai Adam, Wang Xin, Ward Rachel, Witte Philipp, Zhang Cyril, and Zhang Yi. 2023. *Phi-2: The surprising power of small language models*. <https://www.microsoft.com/en-us/research/blog/phi-2-the-surprising-power-of-small-language-models/> [Online; accessed 18-March-2024].
- [34] OpenAI. 2022. ChatGPT. <https://openai.com/blog/chatgpt>.
- [35] R OpenAI. 2023. Gpt-4 technical report. arxiv 2303.08774. *View in Article* 2, 5 (2023).
- [36] Artemis Panagopoulou, Le Xue, Ning Yu, Junnan Li, Dongxu Li, Shafiq Joty, Ran Xu, Silvio Savarese, Caiming Xiong, and Juan Carlos Niebles. 2023. X-InstructBLIP: A Framework for aligning X-Modal instruction-aware representations to LLMs and Emergent Cross-modal Reasoning. *arXiv preprint arXiv:2311.18799* (2023).
- [37] Kishore Papineni, Salim Roukos, Todd Ward, and Wei-Jing Zhu. 2002. Bleu: a method for automatic evaluation of machine translation. In *Proceedings of the 40th annual meeting of the Association for Computational Linguistics*. 311–318.
- [38] Joan Puigcerver, Carlos Riquelme, Basil Mustafa, and Neil Houlsby. 2023. From sparse to soft mixtures of experts. *arXiv preprint arXiv:2308.00951* (2023).
- [39] Zekun Qi, Runpei Dong, Shaochen Zhang, Haoran Geng, Chunrui Han, Zheng Ge, Li Yi, and Kaisheng Ma. 2024. ShapeLLM: Universal 3D Object Understanding for Embodied Interaction. *arXiv preprint arXiv:2402.17766* (2024).
- [40] Zhangyang Qi, Ye Fang, Zeyi Sun, Xiaoyang Wu, Tong Wu, Jiaqi Wang, Dahua Lin, and Hengshuang Zhao. 2023. GPT4Point: A Unified Framework for Point-Language Understanding and Generation. *arXiv preprint arXiv:2312.02980* (2023).
- [41] Nils Reimers and Iryna Gurevych. 2019. Sentence-bert: Sentence embeddings using siamese bert-networks. *arXiv preprint arXiv:1908.10084* (2019).
- [42] Carlos Riquelme, Joan Puigcerver, Basil Mustafa, Maxim Neumann, Rodolphe Jenatton, André Susano Pinto, Daniel Keysers, and Neil Houlsby. 2021. Scaling vision with sparse mixture of experts. *Advances in Neural Information Processing Systems* 34 (2021), 8583–8595.
- [43] Noam Shazeer, Azalia Mirhoseini, Krzysztof Maziarz, Andy Davis, Quoc Le, Geoffrey Hinton, and Jeff Dean. 2017. Outrageously large neural networks: The sparsely-gated mixture-of-experts layer. *arXiv preprint arXiv:1701.06538* (2017).
- [44] Ishika Singh, Valts Blukis, Arsalan Mousavian, Ankit Goyal, Danfei Xu, Jonathan Tremblay, Dieter Fox, Jesse Thomason, and Animesh Garg. 2023. Progprompt: Generating situated robot task plans using large language models. In *2023 IEEE International Conference on Robotics and Automation (ICRA)*. IEEE, 11523–11530.
- [45] Arun James Thirunavukarasu, Darren Shu Jeng Ting, Kabilan Elangovan, Laura Gutierrez, Ting Fang Tan, and Daniel Shu Wei Ting. 2023. Large language models in medicine. *Nature medicine* 29, 8 (2023), 1930–1940.

- [46] Hugo Touvron, Louis Martin, Kevin Stone, Peter Albert, Amjad Almahairi, Yasmine Babaei, Nikolay Bashlykov, Soumya Batra, Prajwal Bhargava, Shruti Bhosale, et al. 2023. Llama 2: Open foundation and fine-tuned chat models. *arXiv preprint arXiv:2307.09288* (2023).
- [47] Ashish Vaswani, Noam Shazeer, Niki Parmar, Jakob Uszkoreit, Llion Jones, Aidan N Gomez, Łukasz Kaiser, and Illia Polosukhin. 2017. Attention is all you need. *Advances in neural information processing systems* 30 (2017).
- [48] Chao Wang, Stephan Hasler, Daniel Tanneberg, Felix Ocker, Frank Joublin, Antonello Ceravola, Joerg Deigmoeller, and Michael Gienger. 2024. Large language models for multi-modal human-robot interaction. *arXiv preprint arXiv:2401.15174* (2024).
- [49] Jason Wei, Xuezhi Wang, Dale Schuurmans, Maarten Bosma, Fei Xia, Ed Chi, Quoc V Le, Denny Zhou, et al. 2022. Chain-of-thought prompting elicits reasoning in large language models. *Advances in Neural Information Processing Systems* 35 (2022), 24824–24837.
- [50] Zhirong Wu, Shuran Song, Aditya Khosla, Fisher Yu, Linguang Zhang, Xiaoou Tang, and Jianxiong Xiao. 2015. 3d shapenets: A deep representation for volumetric shapes. In *Proceedings of the IEEE conference on computer vision and pattern recognition*. 1912–1920.
- [51] Runsen Xu, Xiaolong Wang, Tai Wang, Yilun Chen, Jiangmiao Pang, and Dahua Lin. 2023. Pointllm: Empowering large language models to understand point clouds. *arXiv preprint arXiv:2308.16911* (2023).
- [52] Le Xue, Ning Yu, Shu Zhang, Junnan Li, Roberto Martín-Martín, Jiajun Wu, Caiming Xiong, Ran Xu, Juan Carlos Niebles, and Silvio Savarese. 2023. Ulip-2: Towards scalable multimodal pre-training for 3d understanding. *arXiv preprint arXiv:2305.08275* (2023).
- [53] Aiyuan Yang, Bin Xiao, Bingning Wang, Borong Zhang, Ce Bian, Chao Yin, Chenxu Lv, Da Pan, Dian Wang, Dong Yan, et al. 2023. Baichuan 2: Open large-scale language models. *arXiv preprint arXiv:2309.10305* (2023).
- [54] Senqiao Yang, Jiaming Liu, Ray Zhang, Mingjie Pan, Zoey Guo, Xiaoqi Li, Zehui Chen, Peng Gao, Yandong Guo, and Shanghang Zhang. 2023. Lidar-llm: Exploring the potential of large language models for 3d lidar understanding. *arXiv preprint arXiv:2312.14074* (2023).
- [55] Qinghao Ye, Haiyang Xu, Guohai Xu, Jiabo Ye, Ming Yan, Yiyang Zhou, Junyang Wang, Anwen Hu, Pengcheng Shi, Yaya Shi, et al. 2023. mplug-owl: Modularization empowers large language models with multimodality. *arXiv preprint arXiv:2304.14178* (2023).
- [56] Xumin Yu, Lulu Tang, Yongming Rao, Tiejun Huang, Jie Zhou, and Jiwen Lu. 2022. Point-bert: Pre-training 3d point cloud transformers with masked point modeling. In *Proceedings of the IEEE/CVF conference on computer vision and pattern recognition*. 19313–19322.
- [57] Zhengqing Yuan, Zhaoxu Li, and Lichao Sun. 2023. Tinygpt-v: Efficient multimodal large language model via small backbones. *arXiv preprint arXiv:2312.16862* (2023).
- [58] Ted Zadori, Ahmet Üstün, Arash Ahmadian, Beyza Ermiş, Acyr Locatelli, and Sara Hooker. 2023. Pushing mixture of experts to the limit: Extremely parameter efficient moe for instruction tuning. *arXiv preprint arXiv:2309.05444* (2023).
- [59] Pan Zhang, Xiaoyi Dong Bin Wang, Yuhang Cao, Chao Xu, Linke Ouyang, Zhiyuan Zhao, Shuangrui Ding, Songyang Zhang, Haodong Duan, Hang Yan, et al. 2023. Internlm-xcomposer: A vision-language large model for advanced text-image comprehension and composition. *arXiv preprint arXiv:2309.15112* (2023).
- [60] Peiyuan Zhang, Guangtao Zeng, Tianduo Wang, and Wei Lu. 2024. Tinyllama: An open-source small language model. *arXiv preprint arXiv:2401.02385* (2024).
- [61] Yanzhe Zhang, Ruiyi Zhang, Jiuxiang Gu, Yufan Zhou, Nedim Lipka, Diyi Yang, and Tong Sun. 2023. Enhanced visual instruction tuning for text-rich image understanding. (2023).
- [62] Deyao Zhu, Jun Chen, Xiaoqian Shen, Xiang Li, and Mohamed Elhoseiny. 2023. Minigpt-4: Enhancing vision-language understanding with advanced large language models. *arXiv preprint arXiv:2304.10592* (2023).

A APPENDIX

A.1 Qualitative Results

We present more qualitative results of our MiniGPT-3D, encompassing 3D recognition and captioning, 3D question answering, as well as qualitative comparisons.

A.1.1 3D Recognition and Captioning. Figure 5 and Figure 6 further showcase the qualitative results of our MiniGPT-3D in 3D recognition and captioning. Given a 3D point cloud and instruction, MiniGPT-3D is capable of generating text responses that include the object’s category, quantity, color, and as well as unique characteristics. Furthermore, our MiniGPT-3D also leverages the point cloud information to make reasonable reasoning, deducing potential uses and emergence timelines. This excellent comprehension of point clouds underscores the advantage of employing priors from 2D-LLMs to build 3D-LLMs.

A.1.2 3D Question Answering. Figure 7 further provides the qualitative results of our MiniGPT-3D on 3D question answering. Our MiniGPT-3D supports multi-turn dialogues with users regarding the input 3D point cloud. Users can continuously pose various open-ended questions to MiniGPT-3D about the 3D object, such as its working principle, the number of objects, specific historical event times, and even logical questions. Despite only training 47.8M trainable parameters on one single NVIDIA RTX 3090 GPU for 27 hours, through these examples, we observe that our MiniGPT-3D possesses extensive general knowledge and maintains contextual coherence in multi-turn dialogues, outputting correct text responses. These impressive results underscore the superiority of efficiently aligning 3D point clouds with LLMs based on 2D-LLM knowledge.

A.1.3 Qualitative comparisons. We present more qualitative comparisons, similar to Table 4 in our main paper. The results are shown in Table 13. Compared with other methods, our MiniGPT-3D outputs a more detailed text response, while accurately recognizing object categories and capturing more 3D point cloud information, such as usage, shape, internal components, geometric attributes, materials, etc. The results show the excellent point cloud understanding capabilities of MiniGPT-3D.

A.2 Training Details

This section presents the training details of MiniGPT-3D, encompassing the training settings, model parameter, and the variation in loss across the four training stages.

Training Settings. Table 14 shows the detailed training settings for MiniGPT-3D. Specifically, we use the point-text instruction dataset [51] as the training dataset, encompassing 660k brief captions and 70k detailed captions & conversations. Within this setup, stages I and II employ the brief captions as their training dataset, while detailed captions & conversations are utilized in stages III and IV. Notably, stages III and IV utilize different types of training data from detailed captions & conversations based on a specific sampling ratio. For optimization, we adopt the AdamW optimizer with a weight decay of 0.05 and employ a cosine decay with a linear warm-up learning rate schedule. The initial learning rate gradually decreases as the training stage progresses.

Regarding the hyperparameters of model components, the point cloud encoder is configured consistently with Point-BERT [56], receiving point cloud data inputs of 8192 points. The point cloud projection layer consists of a two-layer MLP network that transforms the 384-dimensional features output from the point cloud encoder to the input dimension of 1408 for the Value and Key layers in Q-Former [27]. Our proposed Mixture of Query Experts (MQE) comprises eight query experts and an expert router. The expert router includes a two-layer MLP network and a softmax operation, outputting the probability distribution for activating the eight query experts. We activate the two experts with the highest probabilities in our experiments. Q-Former consists of 12 blocks, with each attention module containing 12 attention heads. LoRA [21] is used for efficiently fine-tuning the Q-Former, where the rank and alpha of LoRA are set to 8 and 16, respectively. The modality projector consists of a two-layer MLP that transforms the 768-dimensional point cloud queries output from Q-Former to 2560-dimensional point tokens. The large language model backbone comprises 32 blocks. We efficiently fine-tune the LLM using LoRA, with the rank and alpha of LoRA set to 64 and 16, respectively.

Model Parameter. MiniGPT-3D boasts a total of 2.95 B model parameters, yet we only train 47.8 M parameters on a single RTX 3090 (24G) GPU, which took 27 hours. The specific trainable and frozen model modules are detailed in Figure 8a and Table 8b.

Training Loss. Figure 9 shows the changes in loss across the four training stages of MiniGPT-3D. The scale interval on the horizontal axis corresponds to the duration of training. During stage I, though training only point cloud projection layer (MLP), we observe a steady decrease in loss. During stage II, more modules are fine-tuned on the same dataset as stage I, enhancing the model’s learning capacity, and leading to a continued decrease in loss from the end of stage I. During stage III, the introduction of more challenging tasks temporarily increases the loss compared to the end of stage II, followed by a gradual reduction. During stage IV, only MQE is trained. Since the expert router of MQE is trained from scratch, the loss suddenly increases compared to the end of stage III, but then gradually decreases to the same level or even lower.

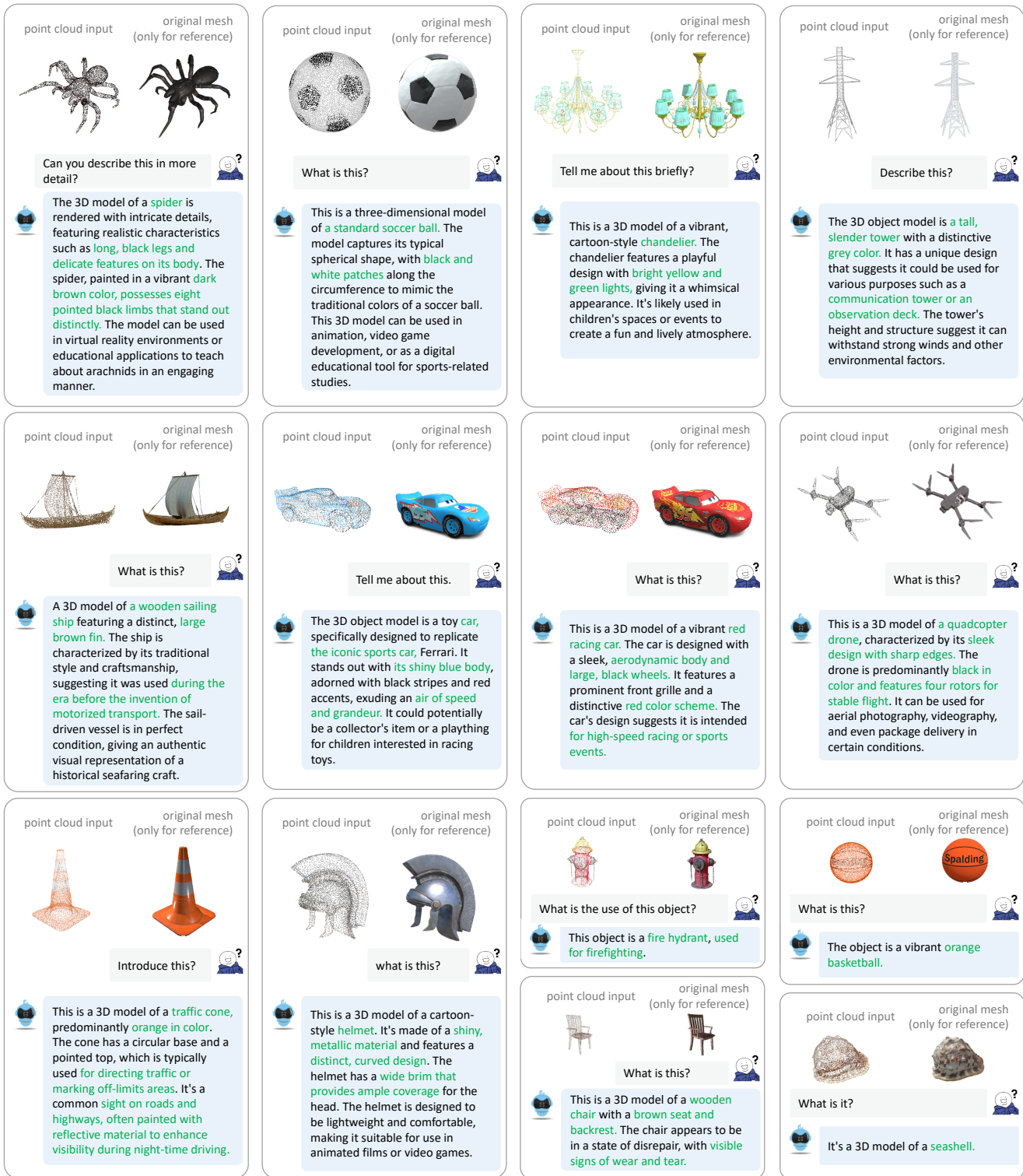


Figure 5: 3D recognition and captioning results (#1) of our MiniGPT-3D. Given a 3D point cloud and a corresponding question, MiniGPT-3D generates a text response. The correct and fine-grained answers are highlight in green.

<p>point cloud input original mesh (only for reference)</p>  <p>Caption this 3D model in detail. </p> <p> The model represents a high-tech rectangular smartphone, showcasing a black and grey exterior with a smooth touch screen. It stands at an impressive height, indicating it's likely to have a large display for multimedia usage like video calling and streaming services. The design of this device suggests it belongs to the leading tech giants, such as Apple Inc., Samsung, or Google.</p>	<p>point cloud input original mesh (only for reference)</p>  <p>Caption this 3D model in detail. </p> <p> The 3D model is of a light, white giraffe with an exquisite mix of brown and black spots on its body. The giraffe's legs are also in white and have prominent grey spots running down each one.</p>	<p>point cloud input original mesh (only for reference)</p>  <p>Describe the object. </p> <p> The object is a 3D model of an old computer with a grey casing, featuring the classic yellow keys on its keyboard. The design exudes nostalgia, hinting at its possible vintage usage or historical significance. Its use in 3D rendering could be for animation, video games, or other digital media, adding a vintage touch to the overall aesthetic.</p>	<p>point cloud input original mesh (only for reference)</p>  <p>Introduce this model. </p> <p> This is a 3D model of a high-end, black and orange pair of athletic shoes. The shoes exhibit a sleek design with thin, slim soles and bold patterns along the sides in contrasting orange. Their color scheme signifies performance footwear, suitable for sports activities or fitness routines. Due to its vibrant color combination, it's also an eye-catching piece for those who are into fashion as well.</p>
<p>point cloud input original mesh (only for reference)</p>  <p>Describe this model. </p> <p> The 3D model is a representation of a tree with green leaves. The tree has a cylindrical trunk and branches that extend in all directions, giving it an organic appearance. It's likely to be used as part of digital environments like video games or animations due to its lifelike design.</p>	<p>point cloud input original mesh (only for reference)</p>  <p>Caption this 3D model in detail. </p> <p> The 3D model is a detailed representation of a lion, with its distinctive brown fur and large, powerful paws. The lion's head is adorned with a long, flowing mane, adding to its majestic appearance. The model is likely used in animations, video games, or as a decorative piece for those who appreciate wildlife.</p>	<p>point cloud input original mesh (only for reference)</p>  <p>Can you walk me through the details of this object? </p> <p> The object is a pair of glasses with a distinct red frame. The lenses are clear, allowing for clear vision. The glasses have a modern design and are likely used for both functional and aesthetic purposes.</p>	<p>point cloud input original mesh (only for reference)</p>  <p>Describe the object. </p> <p> This is a 3D model of an elephant, rendered in a realistic and detailed manner. The model showcases the distinctive features of an elephant, including its large ears, long trunk, and tusks. The model could be used for educational purposes, such as teaching children about different animal species or for creating digital animations or video games.</p>
<p>point cloud input original mesh (only for reference)</p>  <p>Can you explain more about this form? </p> <p> This is a 3D model of a crab, characterized by its vibrant yellow color and the presence of two large claws. The crab's body is segmented, with each segment ending in a claw. The claws are notably large and sharp, which are typical features of crabs for catching prey or defending themselves. This model could be used in various fields such as animation, game design, or marine biology education.</p>	<p>point cloud input original mesh (only for reference)</p>  <p>Provide a detailed description of this model. </p> <p> The 3D model features a vintage-styled black camera. The body of the camera has a glossy black finish, reminiscent of old cameras used during the early 20th century. This kind of camera typically includes an exposure meter, a viewfinder, and two buttons - a shutter button and a release button, making it suitable for manual focusing and adjusting shutter speed. The viewfinder gives users control over when to capture the light in their photographs.</p>	<p>point cloud input original mesh (only for reference)</p>  <p>I want to know what this is, help me. </p> <p> This is a 3D model of a cartoon-style donut, featuring a vibrant yellow color and a pink icing. The donut has a playful, whimsical design that's typical of cartoons. It could be used in animations, video games, or as a decorative item.</p>	<p>point cloud input original mesh (only for reference)</p>  <p>How to learn this musical instrument? </p> <p> You can learn to play this instrument through formal music education, online tutorials, or by practicing with a real-life acoustic guitar.</p>

Figure 6: 3D recognition and captioning results (#2) of our MiniGPT-3D. Given a 3D point cloud and a corresponding question, MiniGPT-3D generates a text response. The correct and fine-grained answers are highlight in green.

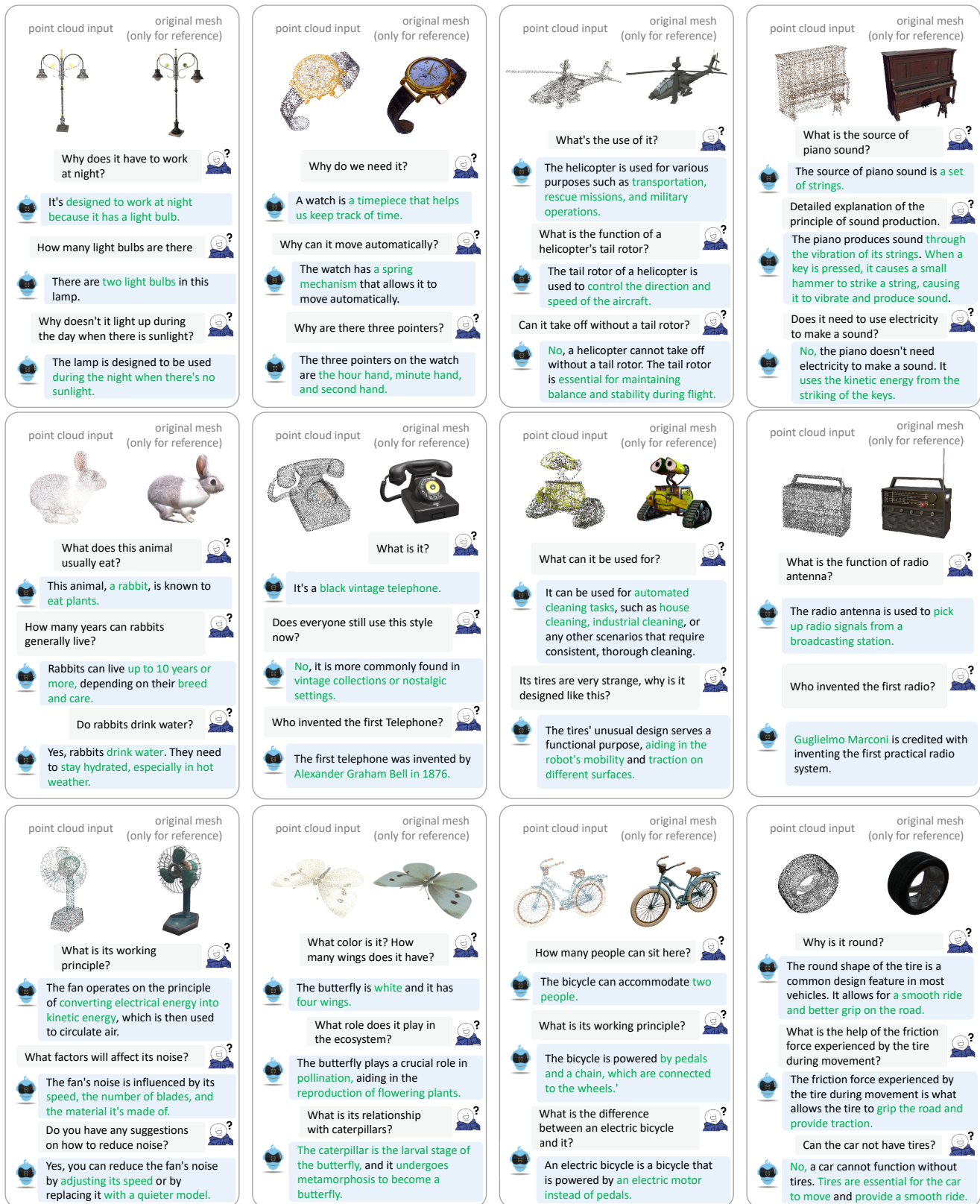


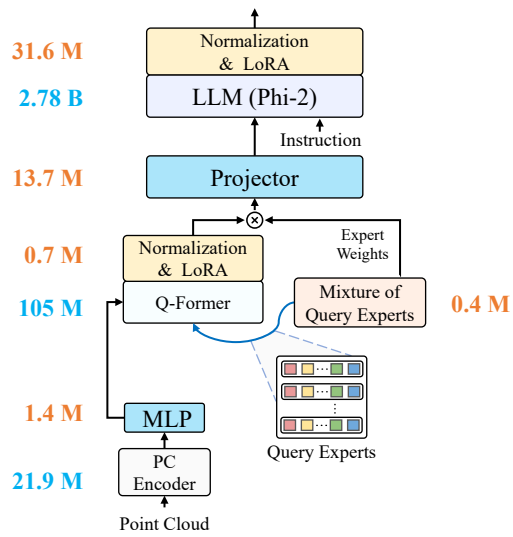
Figure 7: 3D question answering results of our MiniGPT-3D. MiniGPT-3D supports multi-round conversation regarding the 3D object. The correct and fine-grained answers are highlight in green.

Table 13: Qualitative results on ModelNet40. The first image in each sample serves as the input for image-based models, while additional views are provided for reference purposes. Compared to other methods, MiniGPT-3D demonstrates superior accuracy in identifying object categories, capturing richer information, and generating more comprehensive responses.

Samples 1, 2		
Prompt	What is this?	This is an object of
Ground Truth	Sofa	Bed
InstructBLIP-13B [11]	sofa	person cutting meat into small pieces with a large knife
LLaVA-13B[32]	The image is a black and white drawing of a couch.	The image is a black and white depiction of a chair.
Point-Bind LLM [18]	This is a drawing of a person laying on a couch, with a dog nearby.	This is an object of art.
PointLLM-13B [51]	This 3D object is a comfortable, black, three-seater sofa.	This is a model of a neatly made bed, primarily composed of a solid black mattress.
MiniGPT-3D	This is a 3D model of a modern, sleek black sofa. The sofa is designed with a minimalist aesthetic, featuring clean lines and a neutral color palette. It is likely to be used in contemporary interior design, offering comfort and style.	A 3D model of a bed with a black mattress. The bed is characterized by its rectangular shape and the mattress, which is black in color. The bed has a headboard and footboard, both of which are also black. This model can be used in various digital platforms such as video games, animations, or virtual reality experiences.
Samples 3, 4		
Prompt	What is this?	This is an object of
Ground Truth	Guitar	Bottle
InstructBLIP-13B [11]	telescope	wine bottle
LLaVA-13B[32]	The image is a close-up view of a black ink pen sitting on a white surface.	This image features a black and white depiction of a bottle.
Point-Bind LLM [18]	This is a bird flying in the sky.	This is an object of a person holding a bottle of wine.
PointLLM-13B [51]	This 3D model represents a black electric guitar equipped with a distinctive headstock.	This is a 3D model of a bottle, possibly intended for liquids.
MiniGPT-3D	This is a 3d model of a cartoon-style guitar. the guitar is predominantly black in color, with a distinctively large headstock and a long neck. the body of the guitar is also black, and it has a unique design with a large, flat headstock and a long neck. the guitar is likely to be used in animated films, video games, or other digital media.	A 3D model of a bottle, predominantly black in color. The bottle is cylindrical in shape, with a narrow neck and a wide base. The bottle appears to be made of plastic or glass, which is a common material used in the production of bottles. The bottle could be used for various purposes such as storing liquids, serving beverages, or as a decorative item.
Samples 5, 6		
Prompt	What is this?	This is an object of
Ground Truth	Bathtub	Monitor
InstructBLIP-13B [11]	table	the foot
LLaVA-13B[32]	The image features a black and white, close-up view of a grater, which is an object used for grating cheese or other food items.	The image features a small table with a black base and a white or light-colored top.
Point-Bind LLM [18]	This is a bowl or a vase, which is oval-shaped and has a smooth surface.	This is an object of art, a sculpture, or a decorative piece.
PointLLM-13B [51]	The 3D object model represents a realistic, dark grey bathtub.	This is a 3D model of a desktop computer monitor.
MiniGPT-3D	This is a 3D model of a cartoon-style bathtub. The bathtub is predominantly black in color and has a unique design with a curved shape. It is likely to be used in animated films, video games, or children's content.	A 3D model of a sleek, modern black computer monitor. The monitor is rectangular in shape and has a glossy finish, giving it a sleek and professional look. It is equipped with a high-resolution display, suggesting it's suitable for tasks that require high-quality visuals, such as graphic design, video editing, or gaming. The monitor is mounted on a sturdy stand, providing stability and convenience.

Table 14: Detailed training settings.

Setting		Stage I	Stage II	Stage III	Stage IV
Dataset		Point-text Instruction Dataset [51]			
Dataset Types		Brief Caption	Brief Caption	Detailed Caption & Conversation	Detailed Caption & Conversation
Dataset Scale		660 k	660 k	70 k	70 k
Brief Caption	Batch Size	9	9	-	-
	Sample Ratio	1	1	-	-
Detailed Caption	Batch Size	-	-	6	6
	Sample Ratio	-	-	2	2
Single-round Conversation	Batch Size	-	-	10	10
	Sample Ratio	-	-	3	3
Multi-round Conversation	Batch Size	-	-	4	4
	Sample Ratio	-	-	3	3
Max Epoch		1	1	3	1
Iterations Per Training Epoch		70000	70000	10000	10000
Learn Rate Scheduler		linear_warmup_cosine_lr			
Initialized Learn Rate		0.00003	0.00003	0.00001	0.000005
Min Learn Rate		0.00001	0.00001	0.000001	0.000001
Warmup Learn Rate		0.000001	0.000001	0.000001	0.000001
Warmup Steps		7000	7000	3000	1000
Weight decay		0.05	0.05	0.05	0.05
Point Cloud Encoder	Point Number	8192	8192	8192	8192
	Point Group Size	32	32	32	32
	Point Patch	512	512	512	512
	Hidden Size	384	384	384	384
	Head of Attention	6	6	6	6
	Number of Layer	12	12	12	12
Point Cloud Projection Layer	Number of Layer	2	2	2	2
	Dimension	384->768; 768->1408	384->768; 768->1408	384->768; 768->1408	384->768; 768->1408
Mixture of Query Experts	Router Type	-	-	-	Sparse Router [43]
	Top Experts	-	-	-	2
	Number of Query Experts	-	-	-	8
	Number of Expert Router Layer	-	-	-	2
	Dimension of Expert Router Layer	-	-	-	768->256; 256->8
Q-Former	Rank of LoRA	-	8	8	8
	Alpha of LoRA	-	16	16	16
	Number of Layer	12	12	12	12
	Head of Attention	12	12	12	12
	Hidden Size	768	768	768	768
Modality Projector	Number of Layer	2	2	2	2
	Dimension	768->4096; 4096->2560	768->4096; 4096->2560	768->4096; 4096->2560	768->4096; 4096->2560
Large Lanuguage Model Backbone	Rank of LoRA	64	64	64	64
	Alpha of LoRA	16	16	16	16
	Number of Layer	32	32	32	32
	Head of Attention	32	32	32	32
	Hidden Size	2560	2560	2560	2560



(a) Architecture, module parameters of MiniGPT-3D.

Trainable Module	Params	Frozen Module	Params
Point Cloud Projection Layer (MLP)	1.4 M	PC Encoder	21.9 M
Norm & LoRA of Q-Former	0.7 M	Q-Former	105 M
Modality Projector	13.7 M	LLM (Phi-2)	2780 M
Mixture of Query Experts	0.4 M	-	-
Norm & LoRA of LLM	31.6 M	-	-
Total Parameters	47.8 M	-	2907 M

(b) Parameters and trainability of modules in MiniGPT-3D.

Figure 8: Architecture, module parameters, and module trainability of MiniGPT-3D. Blue and orange fonts indicate non-trainable and trainable parameters, respectively.

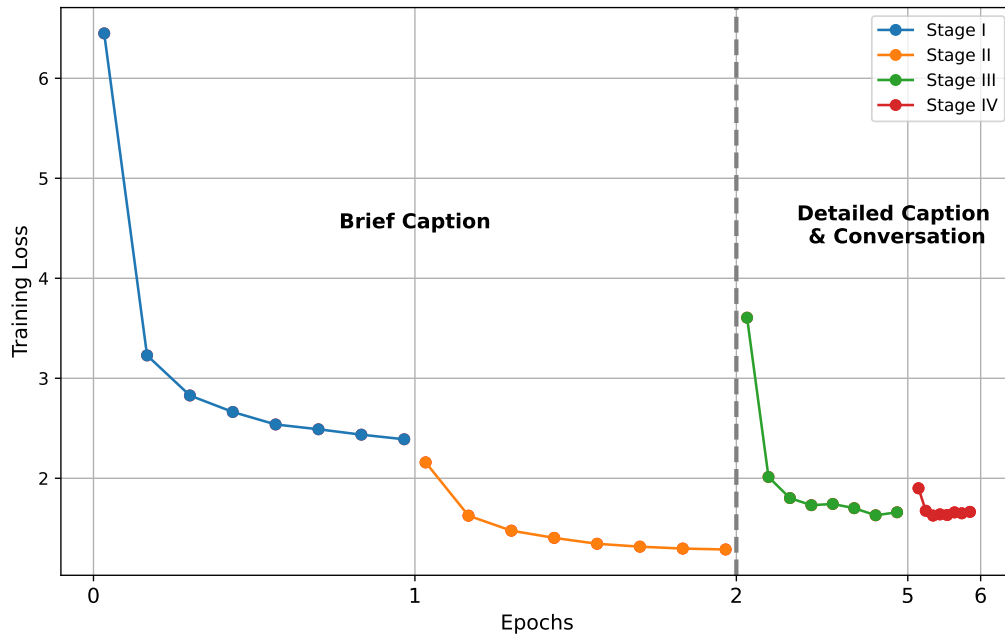


Figure 9: Changes in loss across the four training stages of MiniGPT-3D.